

Spheroid graphite cast iron specimens with defects cracking investigation

M. Leonavičius*, K. Bobyliov, A. Krenevičius***, S. Stupak******

*Vilnius Gediminas Technical University, Saulėtekio al. 11, 10223 Vilnius-40, Lithuania, E-mail: minleo@fm.vgtu.lt

**Vilnius Gediminas Technical University, Saulėtekio al. 11, 10223 Vilnius-40, Lithuania, E-mail: k.bobyliov@fm.vgtu.lt

***Vilnius Gediminas Technical University, Saulėtekio al. 11, 10223 Vilnius-40, Lithuania, E-mail: akren@fm.vgtu.lt

****Vilnius Gediminas Technical University, Saulėtekio al. 11, 10223 Vilnius-40, Lithuania, E-mail: stupakas@adm.vgtu.lt

1. Introduction

In the majority of standards of many countries, only mechanical properties of spheroid graphite iron but not chemical composition are established. According to technological process, every foundry produces cast iron with slightly different microstructure and mechanical properties. This especially concerns the fatigue properties and resistance to cyclic loads [1-4].

Spheroid graphite iron is an engineering material with high strength, fracture toughness and superior wear and abrasion resistance. Its strength and damping properties, lower specific weight, abrasion resistance, high cyclic strength, excellent castability, lower machining cost lets to efficiently replace steel by this material producing mining equipment and transport machines (like big-size gear-wheels and other complex shape parts) and many other applications [1, 5, 6].

Austempered ductile iron (ADI) is a spheroid graphite iron produced using special few stages heat treatment, which comprises the production of ductile cast iron, austenitisation (at about 800-1000°C), followed by quenching to the temperature (about 250-450°C), suitable for the final stage, and isothermal transformation (austempering) of some of the austenitic matrix to other phases before subsequent cooling to room temperature. By varying the heat treatment parameters and changing the obtained microstructure mechanical properties can alter significantly ($\sigma_u = 800\text{-}1600 \text{ MPa}$). By means of casting and thermo-chemical treatment some cast irons are obtained with sufficiently good physical and mechanical properties. Using both the metallurgical and technological means the composition of cast iron is optimized; the intergrain surfaces are cleaned from impurities. While the casting is held at the austempering temperature, nucleation and growth of acicular ferrite occurs, accompanied by rejection of carbon into the austenite. The resulting microstructure, known as "Ausferrite", gives ADI its special attributes. Ausferrite exhibits twice the strength for a given level of ductility compared to the pearlitic, ferritic or martensitic structures formed by conventional heat treatments.

Many machine parts contain initial defects caused by manufacturing process. In casting process, various internal and external defects are met quite often, among them – different voids, which can strongly reduce the strength (durability) of a product [2]. Such inhomogeneity of the material often becomes an origin of fatigue fracture because of elevated local stresses and sensitivity to negative environmental factors.

Due to big dimensions and geometrical complex-

ity of large parts used in mining industry equipment, non-homogeneous parts are obtained quite often. Microstructure anomalies of cast iron and their causes are presented in the work by Goodrich [3]. The anomalies there have been divided into three basic categories: (1) anomalies associated with solidification; (2) anomalies caused by cooling after solidification and treatment; and (3) the catch-all category - „other anomalies“. The most frequent defects are the following: (1) low amount of spheroid graphite; (2) chunky graphite; (3) spiky graphite; (4) chains of spherical graphite gaskets (nodule alignment); (5) vermicular graphite; (6) flake graphite on the surface; (7) small ratio of ferrite/pearlite or pearlite/ferrite; (8) primary carbides; (9) defects of heat treatment; (10) nonmetallic insert; (11) slag insert (dross); and (12) solidification shrinkage and porosity.

Solidification shrinkage and gas porosity are the most common types of casting defects. Porosity can come from gas bubbles entrapped by the molten metal when it is poured into the mould. The shape of these voids is more or less regular.

The shrinkage voids can be separated into two groups according the voids size: (1) macroshrinkage or (2) microshrinkage. Voids appear due to material volume's change during the solidification process. Macroshrinkage voids can be detected by NDE techniques, noted on external surface of the casting or internally after sectioning. Microshrinkage is not so evitable, as soon as the voids size is much lower (from few microns to 0.5 mm); often the voids create a colony. Microshrinkage may appear between grains during solidification. Shrinkage voids are more often in central sections of the casting, wall joints, mould nodes, and are not repairable. All types of voids dramatically reduce the properties of casting performance and durability.

Such defects have a determinative influence on static mechanical properties of cast iron and its resistance to cyclic loads [4]. The evaluation of manufacturing defects in engineering calculations is complicated and forces to increase the used safety factors. In mechanical engineering, specimens with artificially introduced defects are often used for machine part fatigue life analysis. As soon as such method can be used only for machine parts with similar defects, it has natural limits of application [7, 8].

Hence, the influence of different factors on material fatigue strength is still an actual problem. The method which could evaluate the quality of manufactured part and estimate the allowable performance factors, evaluate the influence of detected defects is also required.

2. Testing procedures

The aim of the experiment is to estimate the influence of the defects on spheroid graphite iron cyclic strength.

The object of the investigation is austempered cast iron plate (austenitisation at 950°C, austempering 400°C, 52 min). Chemical composition of the investigated cast iron is as follows: C – 3.3%; Si – 2.5%; Mn – 0.62%; Cr – 0.125%; Mg – 0.045%; Cu – 1.19%; Mo – 0.25; W – 0.60% and Ni – 3.52%. Higher amount of Ni lets to in-

crease the admissible wall thickness producing bigger size parts. According to standard EN 1564, this cast iron is EN-GJS-1000-5.

The group of specimens contains 6 compact specimens (CT). Above them, there are 3 specimens (3, 4, and 5), where external and internal defects were detected – solidification shrinkage voids and gas bubbles formed in casting process. Cylindrical tension specimens were produced seeking to estimate mechanical properties. Table 1 contains values of the obtained static mechanical properties.

Table 1
Mechanical properties of the investigated cast iron

Specimen	E , GPa	σ_{pr} , MPa	$\sigma_{0.2}$, MPa	σ_{us} , MPa	A , %	Hardness, BHN
1	152	422	661	954	1.95	356
2	148 (147)	437	649	995	2.4	360
3	147(159)	438	673	933	1.8	363

Micrograph analysis shows that cast iron has bainite matrix (Fig. 1, a, b, c). Graphite nodules have a shape close to regular spheroid. Nodule size is from 20 to 50 μm , their distribution is quite regular. The matrix contains small amount of retained austenite. Minimal ferrite quantity is typical for such cast iron and bases on heat treatment peculiarities.

Fine grain microstructure assures high strength properties, while the plasticity of ferrite and austenite provides high ductility. The investigated microstructure could be recognized as upper bainite which is obtained using higher heat treatment temperature. Parts manufactured using such cast iron are notable for high strength and fracture

toughness together with quite high relative elongation.

The presence of microvoids is of significance in spheroid graphite iron fracture process studies. The matrix contains microvoids with dimensions about 10-80 μm (Fig. 1, b and c). They were formed between graphite nodules in the late solidification phase, when volume changes are the highest. It should be noticed that as smaller a void is, its shape is more regular. The rate of graphite nodules reaches 300 globules/ cm^2 , and this high index is decreasing the possibility of shrinkage voids appearance. Graphite nodules are surrounded with metallic constituents rich in Si due to segregation.

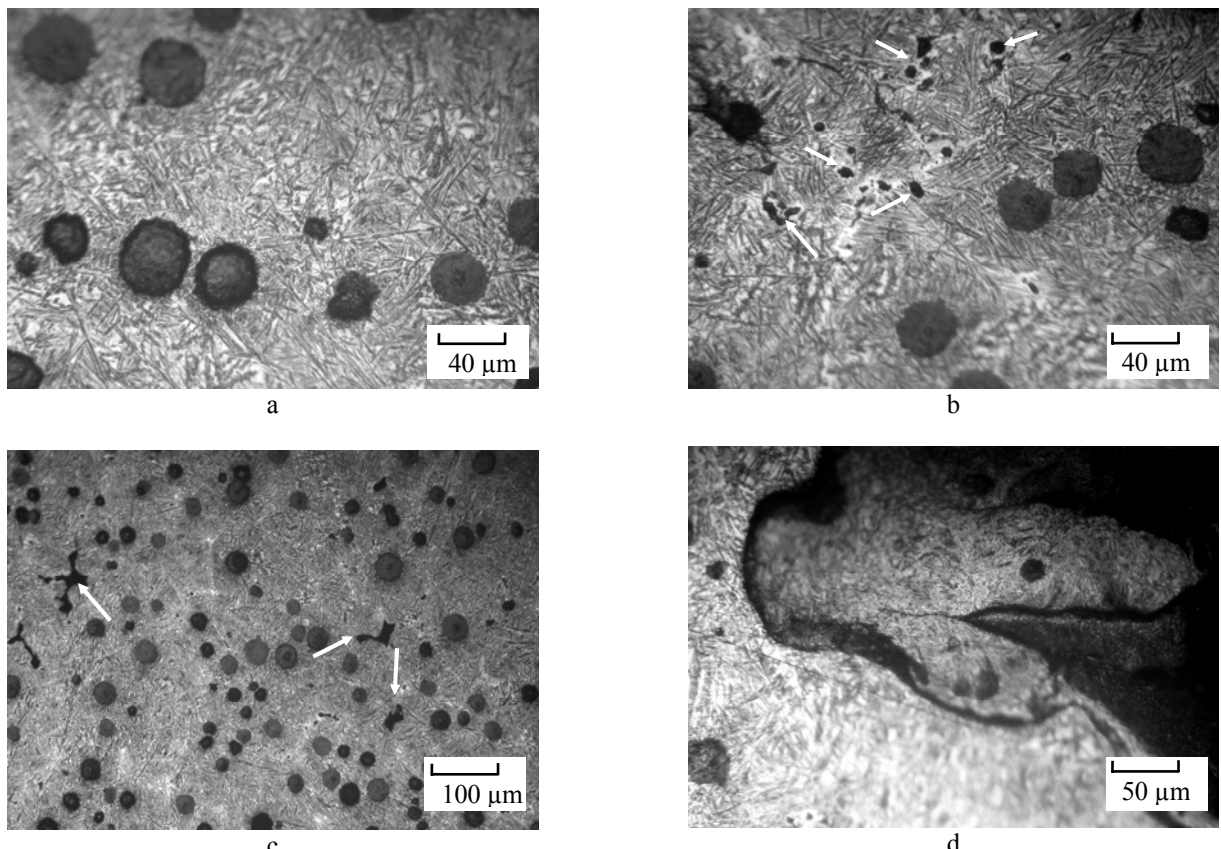


Fig. 1 Cast iron micrograph: a – retained austenite (bright constituents), dark angular constituents (needles) – upper bainite; b, c – shrinkage microvoids (shown with arrows); d – micrograph in the vicinity of a defect

Compact specimens (CT) were prepared; their machined notches were differently directed. Specimen dimensions – $W = 62.5$ mm and $B = 25$ mm.

In order both to define the cyclic strength in cracking and to obtain the dependency of the crack growth rate on stress intensity factor, the method of ASTM E 647-00 was applied. For the calculation of the stress intensity factor K , the following formula was applied

$$\left. \begin{aligned} K &= \frac{F}{BW^{1/2}} f(\lambda) \\ f(\lambda) &= \left[(2+\lambda)/(1-\lambda)^{3/2} \right] \phi(\lambda), \lambda = a/W \\ \phi(\lambda) &= (0.866 + 4.64\lambda - 13.32\lambda^2 + 14.72\lambda^3 - 5.6\lambda^4) \end{aligned} \right\} \quad (1)$$

where F is tension force, a is crack depth, λ is geometrical factor.

The obtained crack growth rate versus stress intensity factor is shown in Fig. 2.

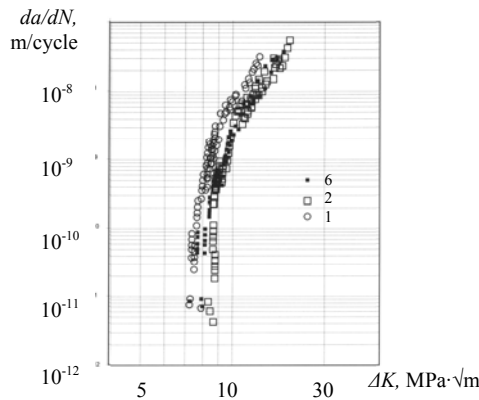


Fig. 2 Dependency of crack growth rate on stress intensity factor for specimens without defects (1, 2, 6)

The obtained crack growth threshold ΔK_{th} reaches $7.2\text{--}8.7$ MPa $\sqrt{\text{m}}$. The values have a noticeable scatter which can be explained by microstructure differences and residual stresses.

Analyzing the specimens with defects (3, 4, 5), it can be noticed that the values of their stress intensity factor can be separated into 2 groups. The first group is formed by crack growth threshold values obtained before the crack reaches the defect. The second group consists of the values, obtained in the area where the crack has already passed the defect.

Using the obtained values, the crack growth rate versus the stress intensity factor for the specimens with defects were estimated (Fig. 3). It was noticed that the values forming the first group are much lower than the ones from the second group. It lets to conclude that a defect has obvious influence on specimen cracking threshold. Additional investigations were accomplished.

The defect in specimen 3 takes 10.4% from total

fracture surface and cracking threshold is $\Delta K_{th} = 7.2$ MPa $\sqrt{\text{m}}$ (crack depth $a < 25$ mm) and $\Delta K_{th} = 8.0\text{--}8.2$ MPa $\sqrt{\text{m}}$, when crack depth $a > 25$ mm (Fig 3, a). In specimen 4 the defect takes 6% from total fracture surface and cracking threshold $\Delta K_{th} = 5.3$ MPa $\sqrt{\text{m}}$ (crack depth $a < 19$ mm), and $\Delta K_{th} = 7.2\text{--}7.5$ MPa $\sqrt{\text{m}}$, when crack depth $a > 25$ mm (Fig. 3, b). In specimen 5, the defect takes 3% of the total fracture surface, the cracking threshold $\Delta K_{th} = 6.1$ MPa $\sqrt{\text{m}}$ (crack depth $a < 23$ mm) and $\Delta K_{th} = 7.5$ MPa $\sqrt{\text{m}}$, when crack depth $a > 23$ mm.

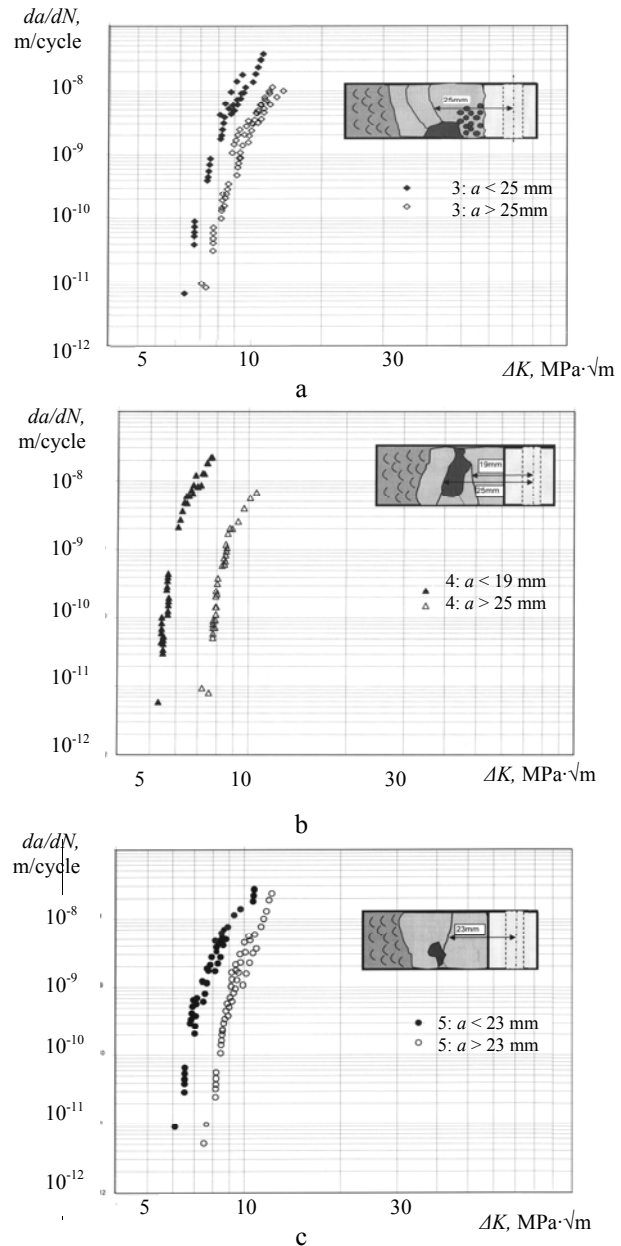


Fig. 3 Dependency of crack growth rate on stress intensity factor for specimens with defects: a – specimen 3; b – specimen 4; c – specimen 5

Table 2

Fracture surface rates

Specimen	Total fracture surface, mm ²	Defect surface, from total, mm ² /%	Static fracture surface, from total, mm ² /%	Fatigue fracture surface, from total, mm ² /%	Defect surface from fatigue fracture, %
3	994	100 / 10.4%	408 / 41%	586 / 59%	17.1
4	944	60 / 6%	462 / 49%	482 / 51%	12.5
5	955	28.6 / 3%	340 / 35.6%	615 / 64.4%	8.4

3. Analytical study

Defect zone should not be treated as an empty space. Often, defect zone consists of a few irregular shape voids which are separated with thin walls that have a certain influence on crack growth. The shape of some defects is crack-like; so, the defect can be described by fracture mechanics, and the defect can be regarded as a crack which starts to grow if the range of applied stress intensity factor exceeds its threshold value. In order to investigate the influence of the defects on crack propagation, additional analytical study of test results for specimens with defects was done.

As we see on Fig. 3, graphic dependencies have two noticeable zones with higher (after crack passes the defect) and lower (before crack reaches the defect) ΔK values. The difference between them depends on defect size, and reaches from 10% for specimen 4 to 20% for specimen 5.

In order to evaluate the influence of a defect on the fracture geometrical indices, the method, presented in [6], was applied. Using optical scanning, obtained fracture surface views were post processed in AutoCAD and defect surface was estimated.

First, boundaries of the defect and the crack front stopping marks ("beachmarks") are estimated. Analyzing the beachmarks on specimen 5 fracture surface (Fig. 4, a), they were traced marking their intersections with specimen surface with identical numbers ("1-1", "2-2", etc.). It was noticed that after reaching the defect the greatest part of the beachmarks were joined in the vicinity of the defect (on the right side of the fracture); contrarily, they rested separated in the specimen part with no defect (on the left side). This feature could be explained by microstructure inhomogeneity in the vicinity of the defect. Also, the difference in position of the outer points of the beachmarks was respectable.

Second, such geometrical indices as the defect surface, the moment of inertia, the influence on fracture geometrical indices are calculated, using additional software (used calculation scheme is presented in Fig. 4, b). The indices are calculated for each beachmark, so a sequence of values is obtained according to varying crack depth.

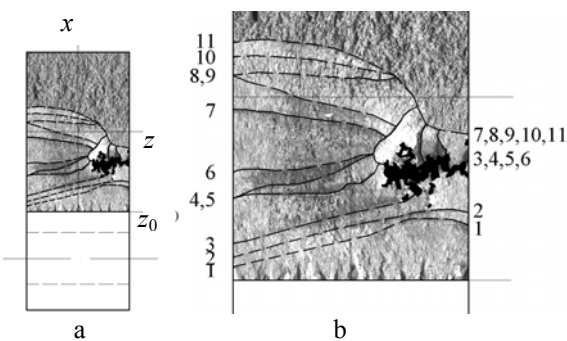


Fig. 4 Specimen 5 section geometrical indices calculations:
a – specimen with defect common view; b – beachmarks (bolded lines)

Geometrical indices are calculated according to the formulas

$$\left. \begin{aligned} A &= (W - a)B, \quad I = B(W - a)^3 / 12 \\ S &= I / e_c, \quad A^* = \sum A_i^*, \quad I^* = \int_A y_i^2 dA_i^* \\ A_d &= A - A^*, \quad S_d = I / e_{cd} \\ I_d &= I + A(e_c - e_{cd})^2 - (I^* + A^*(e^* - e_{cd}))^2 \\ e_c &= (W - a) / 2, \quad e^* = \sum A_i^* y_i / A^* \\ e_{cd} &= e_c + A^*(e^* - e_c) / A_d, \quad i = 1, 2, \dots, n \end{aligned} \right\} \quad (2)$$

where A , I , S are accordingly section area, moment of inertia, and section modulus of fracture with defects (n is the number of defects) without assessment of defects; A_d , I_d , S_d are correspondingly section area, moment of inertia, and section modulus of fracture with defects with assessment of defects; A^* , e^* and I^* are correspondingly area and its centroid distance from crack front and moment of inertia about centroid axe z of CT fracture defects obtained by AutoCAD; e_c and e_{cd} are CT fracture surface centroid distance from the crack front without assessment of defects and with assessment of defects correspondingly.

Nominal normal stress at the crack tip is calculated in the following way

$$\sigma = \left(\frac{2F}{BW} \right) \frac{(2 + \lambda)}{(1 - \lambda)^2} \quad (3)$$

By inserting this expression into formula (1) the following formula for calculating the stress intensity factor is obtained

$$K_d = 0.5\sigma W^{1/2} (1 - \lambda)^{1/2} \phi(\lambda) \quad (4)$$

The real nominal stresses differ from the calculated ones according formula (3) because the geometric indices are lower due to defects in the fracture. With regard to changing geometric indices, the real nominal stresses are calculated in this way

$$\sigma_d = F / A_d + M / S_d \quad (5)$$

where A_d is real area of the cross-section, S_d is real section modulus. By putting the results of expression (5) into (4), it is possible to calculate the real stress intensity factor

$$K_d = 0.5\sigma_d W^{1/2} (1 - \lambda)^{1/2} \varphi(\lambda) \quad (6)$$

Therefore, the obtained stress intensity factor threshold ΔK_{th} of specimens with defects is conventional because a presumption is made that the crack is perpendicular to normal stresses. But it should be mentioned that the results obtained with three CT specimens with defects are similar.

Using the result of experiment, by post-processing the stress intensity factor according to formula (6), the new dependency between crack growth ratio and stress intensity factor range was estimated for defective specimens. These calculations help to evaluate the influence of the defect and to obtain the new ΔK_{th} values even for defective specimen. On the other side, the defect influence on cyclic strength becomes more evident.

4. Fracture surface analysis

Due to material properties, noticeable tunnelling effect was not found. Nevertheless, the main crack front in some specimens, especially in containing defects, is curved; and this is a witness of fatigue crack propagation sensitivity to stress triaxility. It should be noticed that the defect does not become a reason of sudden fracture. Analyzing specimen 5, we can notice, that the crack front often

grows faster in the direction of the defect, later joins it, but after passing the defect the crack grows slower than in the next zone without defect (Fig. 5).

In the vicinity of the defect graphite nodules alignments and microvoids were found. They create conditions for microcrack appearance and propagation while the main crack is close to the defect. Initiated secondary cracks around the defect later join the main crack, creating complicated crack propagation scene.

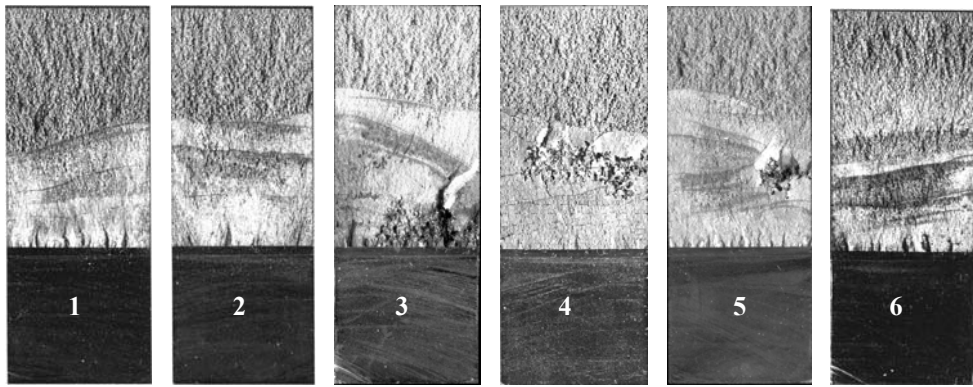


Fig. 5 Specimen fracture surface views

The fatigue fracture surface makes from 50 to 70 % of the total fracture surface. For detailed fractography analysis specimen 5 has been chosen. Comparing to other specimens fractures, this one has significant differences caused by defect influence.

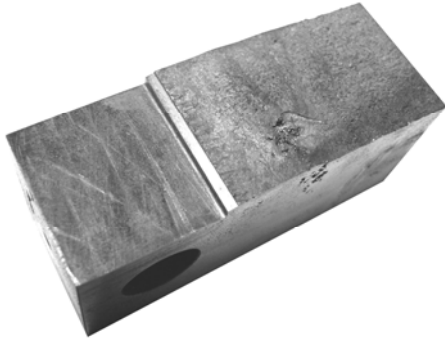


Fig. 6 Half of specimen 5 after fracture

Fracture surface examination allows making an assumption that the examined fatigue fracture is brittle and has common tensile loading mode signs. The specimen has no obvious plasticity features, such as cross-section changes or „shear lips“. The fracture plane, which is close to specimen symmetry plan and is perpendicular to maximum tension stresses, is typical for brittle fracture.

According to the testing procedure, crack stopping marks appear when cyclic load is reduced causing the diminution of the crack growth striations. So, on the macroscopic level, it results in both surface roughness and color changes. This process is explained in dislocation and slipping occurring in crystals [6]. In such way, crack stopping marks are related to lower ΔK values, which are close to cracking threshold ΔK_{th} .

Analyzing fracture surfaces containing defects, it should be useful to pay attention to the shape and direction of crack stopping marks, as soon as it can give signs

about the changes in crack propagation. It is noticeable that in the beginning the crack propagates faster in the right side of the cross-section (Fig. 4, b and Fig. 7), comparing to the left side. An assumption was made that total influence of the defect geometry causes this difference. As it was calculated before, the centroid of a cross-section was displaced causing the more complex eccentric bending, when one of the sides has higher load (i.e. stresses and stress intensity factor) than the other.

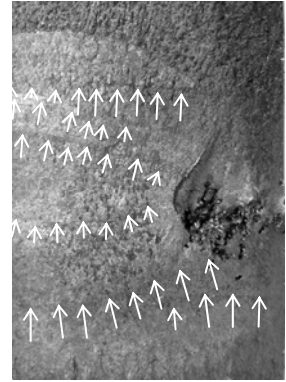


Fig. 7 Crack front stopping marks (specimen 5). Arrows show the direction of crack propagation

When the crack reaches the defect, stopping marks are close to perpendicular line of the specimen outer surface (on the left) and combines on the right (Fig. 7). After passing the defect, the crack propagates faster on the side without defect. Contrarily, the defect is led with microstructure anomalies and grain orientation discrepancies which decrease the crack growth rate on the right side of the specimen.

Crack propagation is affected by several factors, changing the crack growth mechanism: local microstructure changes, stress intensity factor and strain state alteration due to defects, and strain state change.

5. Conclusions

1. Microstructure analysis shows that detected casting defects are shrinkage voids and gas bubbles.
2. Section geometrical indices (i.e. surface, static and inertia moments) depend on defect size and its position.
3. The defined cracking threshold ΔK_{th} in CT specimen without defects varies from 7.2 to 8.7 MPa \sqrt{m} . The cracking threshold of CT specimens with defects varies from 5.3 to 8.2 MPa \sqrt{m} .
4. Different cracking threshold values are obtained for specimens with defects, when the crack growth rate is $v = 10^{-10} - 10^{-12}$ m/cycle.
5. Defects have significant influence on crack propagation trajectory.

References

1. **Dorazil, E.** High Strength Austempered Ductile Cast Iron.-New York: Ellis Horwood, 1991.-250p.
2. **Budinski, K.G., Budinski, M.K.** Engineering Materials. Properties and Selection.-Pearson: Prentice Hall, 2005.-885p.
3. **Goodrich, G.M.** Cast iron microstructure anomalies and their cause. AFS Transactions. American Foundry Society.-Illinois: Inc., Des Plaines, 1997, p.669-680.
4. **Daunys, M., Putnaitė, D.** Determination of lifetime for railway carriages automatic coupler SA-3.-Mechanika. -Kaunas: Technologija, 2005, No.2(52), p.5-10.
5. **Leonavičius, M.K., Petraitis, G., Šukšta, M., Svalbonas, V.** Strength of mills and crushers equipment materials subjected to gigacycle loading.-J. of Civil Engineering and Management. -Vilnius: Technika, 2006, v.12, No2, p.135-141.
6. **Stupak, S., Leonavičius M.K., Bobyliov, K.** Section properties of fracture of compact specimen with defects. -Proc. of 11th Int. Conf. "Mechanika 2006". -Kaunas: Technologija, 2006, p.335-339.
7. **Jokūbaitis V.** Regularities in propagation of opened corrosion-induced cracks in concrete.-J. of Civil Engineering and Management. -Vilnius: Technika, 2007, v.13, No2, p.107-113.
8. **Krenevičius, A., Leonavičius, M.K., Petraitis, G., Gutauskas, M., Stonkus, R.** Strength of differently cooled cast iron subjected to cyclic loading. -Mechanika. -Kaunas: Technologija, 2007, No.4(66), p.18-22.

M. Leonavičius, K. Bobyliov, A. Krenevičius, S. Stupak

STIPRIOJO KETAUS BANDINIŲ SU DEFEKTAIS PLEIŠĖJIMO TYRIMAS

R e z i u m ē

Pateikiami duomenys apie ketaus su defektais pleišimo slenksčio eksperimentinį ir analitinį tyrimą. Nustatyti stipriojo ketaus mechaninių savybių rodikliai ($\sigma_u \simeq 950$ MPa) ir mikrostruktūra. Išbandyti CT bandiniai iš ketaus be defektų ir ketaus su defektais. Sudarytos priklausomybės tarp plyšio plitimo greičio ir įtempių intensyvumo koeficiente intervalo bandiniams su tuščių tipo defektais ir be jų. Gautos pleišimo slenksčio ΔK_{th} reikšmės, kai plyšio plitimo greitis $v = 10^{-10}$ m/ciklą, $v = 10^{-11}$ m/ciklą ir $v = 10^{-12}$ m/ciklą.

M. Leonavičius, K. Bobyliov, A. Krenevičius, S. Stupak

SPHEROID GRAPHITE CAST IRON SPECIMEN WITH DEFECTS CRACKING INVESTIGATION

S u m m a r y

The results of experimental and analytical study of cracking threshold for cast iron with defects have been presented. The mechanical properties indices ($\sigma_u \simeq 950$ MPa) and microstructure of spheroid graphite iron have been estimated. CT specimens from cast iron with defects and cast iron without defects have been tested. Dependencies between crack growth rate and threshold for specimens with shrinkage voids and without them have been obtained. Threshold values are obtained when the crack growth rate is $v=10^{-10}$ m/cycle, $v=10^{-11}$ m/cycle and $v=10^{-12}$ m/cycle.

М. Леонавичюс, К. Бобылёв, А. Кренявичюс, С. Ступак

ИССЛЕДОВАНИЕ ТРЕЩИНОСТОЙКОСТИ ОБРАЗЦОВ ИЗ ВЫСОКОПРОЧНОГО ЧУГУНА С ДЕФЕКТАМИ

Р е з ю м е

Представлены данные экспериментального и аналитического исследования порога трещиностойкости чугуна с дефектами. Определены характеристики механических свойств ($\sigma_u \simeq 950$ MPa) и микроструктура высокопрочного чугуна. Проведены эксперименты с компактными образцами из чугуна без дефектов и чугуна с дефектами. Установлены зависимости между скоростью распространения трещины и коэффициентом интенсивности напряжений для образцов с пустотообразными дефектами и без них. Получены значения порога трещиностойкости при скоростях распространения трещины $v = 10^{-10}$ м/цикл, $v = 10^{-11}$ м/цикл и $v = 10^{-12}$ м/цикл.

Received November 19, 2007